



Indian Ocean Dipole affects eastern tropical Atlantic salinity through Congo River Basin hydrology

Sreelekha Jarugula ¹✉ & Michael J. McPhaden ²

The Indian Ocean Dipole is associated with a pronounced sea surface temperature gradient between eastern and western Indian Ocean. Here, we describe a striking contrast in Congo basin rainfall, river discharge and Eastern Tropical Atlantic surface salinity linked to the recent strong 2019 positive Dipole event and strong 2016 negative Dipole event. The sea surface temperature gradient across the Indian Ocean during the 2019 positive event drove tropospheric circulation changes that led to an increase in moisture convergence and convection over the Congo basin and an increase in Congo River discharge that was later reflected in a decrease in eastern tropical Atlantic surface salinity in early 2020. Opposite tendencies were observed in association with the 2016 negative event. This sequence of linkages is shown to apply more generally to Dipole events over the past several decades and thus represents a source of predictability for forecasting Congo basin hydrology and eastern tropical Atlantic oceanic conditions.

¹Jet Propulsion Laboratory, California Institute of Technology, Pasadena, CA 91109, USA. ²NOAA Pacific Marine Environmental Laboratory, Seattle, WA 98115, USA. ✉email: sreelekha.jarugula@jpl.nasa.gov

The Congo River Basin (CRB) in central Africa spread across 3.7 million km² is the second largest river system in the world¹ and a major source of terrestrial organic carbon² and dissolved iron³ to the Atlantic Ocean. The CRB is one of the major convective zones in the tropics with an annual precipitation of 1100–1900 mm and has a profound influence on the regional climate by impacting hydrological and biogeochemical cycles^{4,5}. Owing to the movement of the Inter Tropical Convergence Zone (ITCZ), the Congo River discharge (CRD) is bimodal with a main maximum peak during November–December, a secondary maximum during April–May and minima during March and August^{4,6–8}. The river outflow is known to drive the seasonal changes in sea surface salinity (SSS) in the Eastern Tropical Atlantic (ETA) which can impact the variability in sea surface temperature (SST), local climate of eastern equatorial Atlantic and aid the onset of the West African Monsoon^{8–12}. Despite its importance, the CRB is one of the least studied continental river basins in the world due to lack of observational data^{13,14}.

The Indian Ocean Dipole (IOD) is a prominent climate mode in the tropical Indian ocean associated with coupled ocean–atmosphere interactions that affect the regional climate and lives of millions of people in the surrounding countries^{15–17}. The Dipole Mode Index (DMI), estimated as the difference in the SST anomalies between the eastern (90°E–110°E, 10°S–0°N) and western (50°E–70°E, 10°S–10°N) equatorial Indian ocean, is used as a measure of the strength of IOD¹⁴. A positive IOD event (p-IOD) is associated with warm SST anomalies in the western equatorial Indian Ocean, cold SST anomalies in the eastern Indian Ocean, and reversal of the usual westerlies in the equatorial Indian Ocean. These conditions often result in enhanced monsoon rainfall over the Indian subcontinent, catastrophic floods in the eastern Africa^{18,19}, droughts in southern Africa²⁰, severe droughts and wildfires in southeast Asia²¹ and Australia^{22,23}. A negative IOD (n-IOD) event on the other hand has roughly opposite signed anomalies in the Indian Ocean and opposite climatic impacts compared to a positive IOD event. The IOD usually develops during boreal summer (June–August) with a peak phase in autumn (September–November) and decay in the following winter²⁴. Several studies have linked the development of IOD to El Niño/Southern Oscillation (ENSO) but there are many instances when IOD events occur independently of ENSO¹⁹. For example, the extreme n-IOD in 2016 (Fig. 1a) and p-IOD in 2019 (Fig. 1b) occurred while the tropical Pacific Ocean was in a weak La Niña and a neutral state respectively^{25,26}. The DMI associated with these two IOD events exceeded 2 standard deviations (Fig. 1c). However, so as to not conflate IOD impacts with ENSO forced variability, we linearly remove the Niño3.4 index from the DMI using orthogonal regression prior to our analyses (see Methods section). The differences with and without ENSO linearly removed are small (Supplementary Fig. S1) in any case, but procedure ensures we are cleanly isolating IOD impacts.

The CRD measured at the Kinshasa–Brazzaville station, about 500 km upstream of the river mouth, provides an estimate of the outflow for over 98% of the CRB^{4,27}. The peak CRD during December–January is observed to be significantly lower than normal (<1 standard deviation) during the extreme n-IOD in 2016 and much higher than normal during the extreme p-IOD in 2019 (Fig. 1d). Thus, the boreal winter maximum in CRD is strongly influenced by the IOD. A composite analysis which includes 11 p-IOD events and 14 n-IOD events selected based on the criteria that DMI exceeds at least ±1 standard deviation during 1954–2020 shows increased winter-time discharge during positive IOD events (Supplementary Fig. S2). However, the difference in the winter-time discharge is more pronounced during extreme positive and negative IOD years. The highest and lowest

winter-time discharge for the Congo River was recorded following extreme positive and negative IOD events in 1961 and 1958 (Supplementary Fig. S2), respectively, neither of which was influenced by ENSO^{28,29}. The Congo River is a major source of freshwater, critical for the livelihood of people dependent on irrigation and fisheries in CRB. Severe drought or flooding of the tributaries can cause serious damage to infrastructure, food production, drinking water supplies and disruption to the lives of millions of people³⁰. Hence it is important to understand the climate phenomena that impact the hydrology and river outflow in the Congo Basin. In this study, the effect of IOD events on the Congo River outflow and the sea surface salinity in the ETA is studied for the first time with the use of several in situ, satellite and reanalysis data sets. We describe the mechanisms through which the IOD affects the Congo basin hydrology by presenting a detailed analysis for the extreme n-IOD in 2016 and the extreme p-IOD in 2019. We then examine the relationship between DMI, CRB Rainfall and Congo River discharge based on a statistical analysis of data for all the years during the period 1985–2019 so as to generalize our results to other IOD events.

Results and discussion

Indian Ocean Dipole and Congo basin rainfall. The boreal autumn (September–November) rainfall over East Africa and Central Africa is dynamically linked to the varying SST patterns over the Indian ocean and weakly related to changes in the Pacific Ocean^{31,32}. During a p-IOD, warming of the western Indian ocean and changes in wind circulation cause an eastward shift of the Mascarene High allowing a huge influx of moisture into eastern tropical Africa³¹ north of the Mozambique Channel²⁰ resulting in wet conditions and extreme floods. On the other hand, a p-IOD induces divergent and anti-cyclonic circulation over southeastern Africa resulting in drier than normal conditions there. The SST anomalies in the western Indian Ocean and the DMI can thus be used as potential predictors for the tropical East African rainfall³³.

While the effects of the IOD on the East African rainfall and its impacts on food security of the region are relatively well understood³⁴, this study is mainly focused on understanding the relation between the IOD, Congo Basin rainfall and their further connections to Congo River discharge and ETA SSS. Elements of these linkages have been described before^{32,35} but the end-to-end connection between the Indian and Atlantic Oceans through Africa has not been clearly documented. For the 2016 and 2019 IOD events that we are highlighting, the biggest difference in CRB rainfall occurred in October (Fig. 2a). Moreover, October 2019 was the wettest October since the start of the blended satellite-in situ TAMSAT rainfall record in 1983 (Supplementary Fig. S3). These extreme rains over the Congo Basin led to above normal Congo River discharge (Fig. 1 and Supplementary Fig. S2) and the worst flooding in the Democratic Republic of Congo in 50 years³⁰. October to December 2019 was also a period of extreme rainfall and flooding in East Africa related to the IOD that year³⁶.

The precipitation average over the Congo Basin in October 2019 was 38% higher in TAMSAT rainfall and 26% higher in GPCP rainfall than in 2016. This result is consistent with regression analysis between October DMI and CRB rainfall over the past 35 years that suggests increased precipitation during a positive dipole year and decreased precipitation during a negative dipole year (Fig. 2b, c). The difference in October rainfall between positive and negative IOD years is lower for GPCP possibly due to the fact that its spatial resolution is 10 times lower, which may miss important local extrema (Supplementary Fig. S4). Cross-correlation between the Niño3.4 index and CRB rainfall shows a

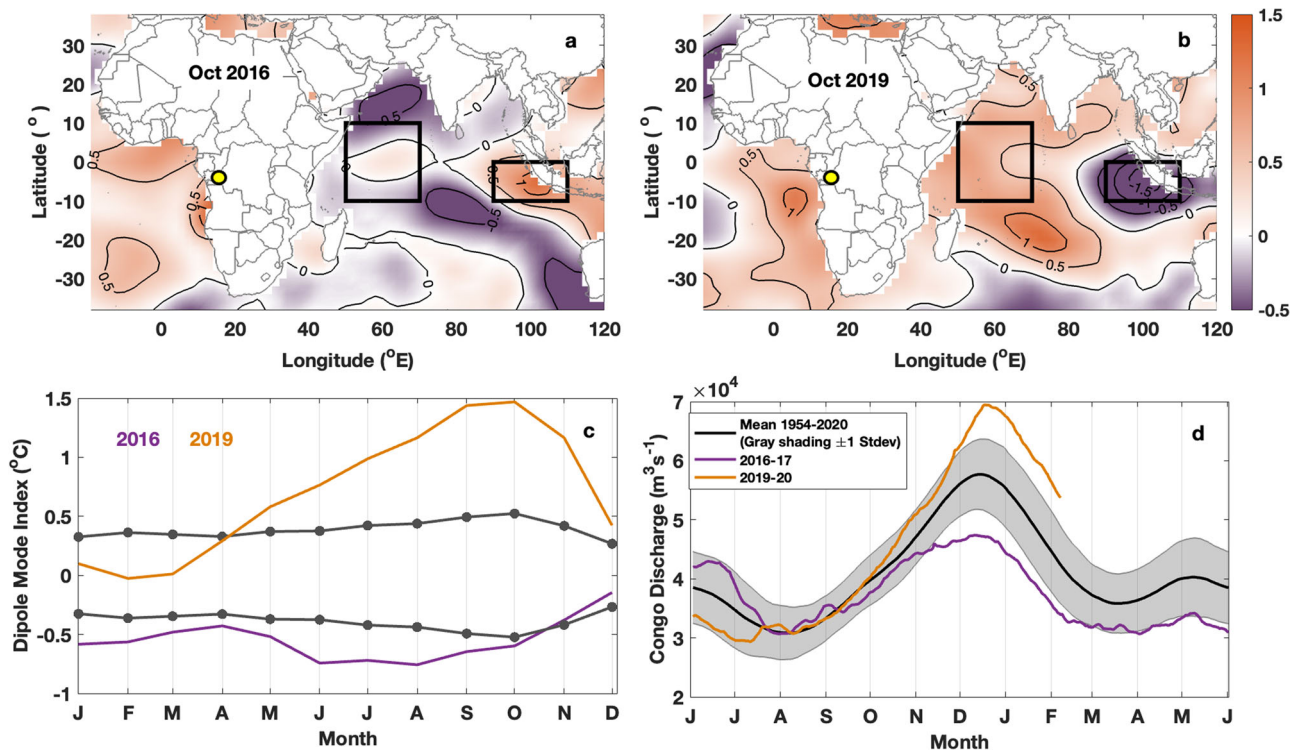


Fig. 1 Effect of Indian Ocean Dipole on Congo River Discharge. NOAA ERSST monthly sea surface temperature anomaly (color; °C) in October (a) 2016 and (b) 2019 relative to the October SST climatology during 1991–2020. c Dipole Mode Index (DMI; °C) estimated from NOAA ERSST during 2016 (purple) and 2019 (orange) with ± 1 monthly standard deviation (dotted gray lines) for period 1950–2021. DMI calculated as SST anomaly difference between the eastern (10°S–0°N, 90°E–110°E) and western (10°S–10°N, 50°E–70°E) equatorial Indian Ocean (black boxes marked in a and b) and the Niño.3.4 index has been linearly removed via orthogonal regression analysis. d Daily Congo River discharge (m^3s^{-1}) measured at the Kinshasa–Brazzaville station during 2016–17 (purple) and 2019–20 (orange); mean river discharge (black) and ± 1 standard deviation (gray shading) is estimated during 1954–2020. Kinshasa–Brazzaville station location (yellow circle) marked in a and b.

positive dependence of East African rainfall on ENSO, but no significant correlation with CRB rainfall during October (Supplementary Fig. S5) so there are no confounding influences from the Pacific to obscure the IOD impacts on CRB rainfall at this time^{37–40}. In addition, the DMI in July–September is significantly correlated with the following October CRB rainfall (Supplementary Fig. S6a, b), the lead time of which represents a source of seasonal predictability for rainfall over west Africa based on the phase of the IOD.

Atmospheric moisture budget. Having identified the statistical linear relationship between DMI and CRB rainfall, we next examine the atmospheric moisture budget to better understand the physical processes that underpin the relationship. The contrasting SST anomalies in the eastern and western Indian Ocean associated with IOD drive changes in the large-scale tropospheric circulation over the tropical belt spanning Africa to Indonesia^{18,19,32,37}. In October 2016, precipitation and relative humidity were enhanced over the eastern Indian Ocean owing to warm SST anomalies there (Fig. 3a, c). The anomaly maps of rain and 850 hPa winds show low-level convergence of moisture in the eastern Indian Ocean, while 300 hPa winds depict an upper-level divergence over the eastern Indian Ocean. Both 850 hPa and 300 hPa wind circulation are weak over the CRB with 300 hPa relative humidity of about 50% less in 2016. On the other hand, in October 2019 the precipitation rate over CRB increased accompanied by a significant increase in relative humidity at 300 hPa pressure level over the region (Fig. 3b, d). Strong easterlies at the 300 hPa pressure level transported significant amount of moisture

from the eastern to the central Indian Ocean and the Congo basin.

A detailed atmospheric moisture budget analysis is performed to understand October precipitation over Congo Basin in 2016 and 2019 (Fig. 4). During October 2016, a lot of moisture convergence occurs in the eastern equatorial and southern Indian Ocean which leads to wet conditions to the east of 90°E while drier conditions prevail over Africa (Fig. 4a–c). On the other hand, in October 2019 moisture convergence is intensified over the central equatorial Indian Ocean, western Indian Ocean and over central Africa (Fig. 4d–f). The increased precipitation and moisture supply to the CRB in October 2019 is not due to local rate of change of water vapor but mainly driven by moisture convergence over the region in addition to the transport of moisture by the upper-level easterly jet from the central and western Indian Ocean. These results align with previous studies that find the Indian Ocean to be a major source of moisture supply for rainfall over the Congo basin during September–November^{19,31,32}.

Indian Ocean Dipole affects Congo River discharge. The Congo River is mainly fed by precipitation occurring over the CRB throughout the year. The rain water collected across the northern Congo Basin in the several tributaries and streams takes about 1–3 months to reach the Brazzaville/Kinshasa station where the river discharge is measured (Fig. 1d). The tributaries across the north and central Congo Basin contribute significantly to the boreal winter peak in the discharge and the southern basin tributaries lead to secondary peak in the discharge during March–April⁴¹.

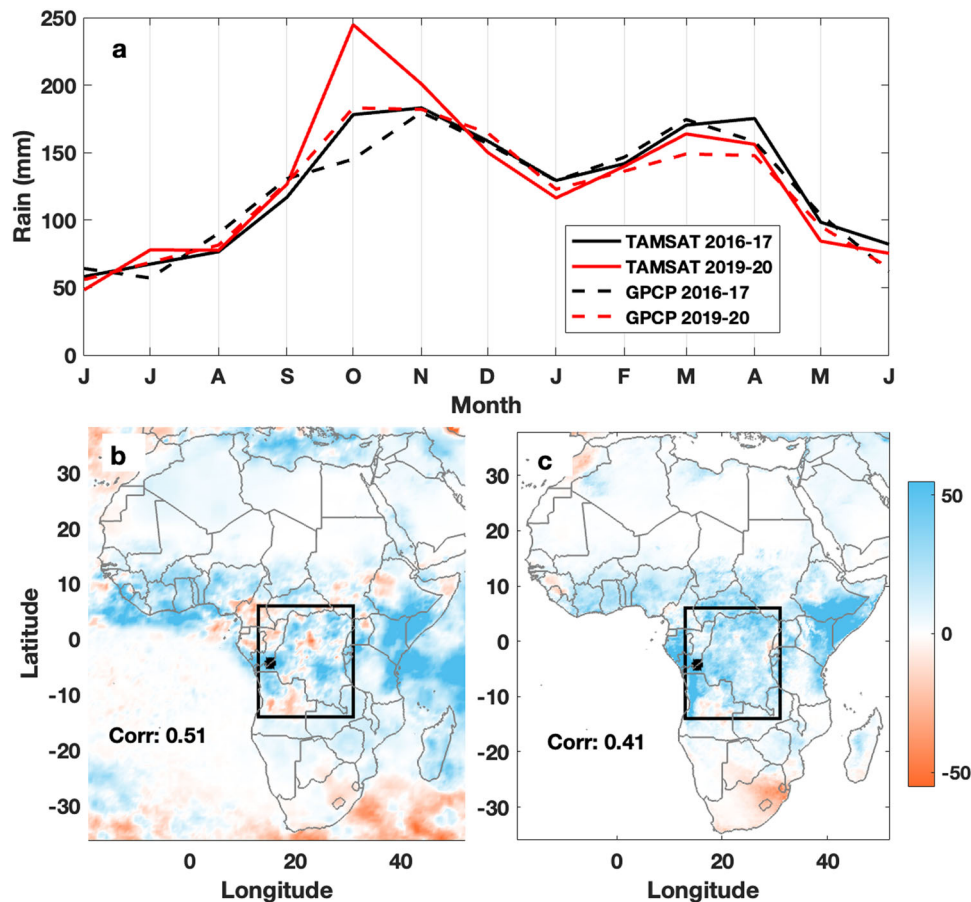


Fig. 2 Relation between Dipole Mode Index (DMI) and Congo River Basin (CRB) Rainfall. **a** Mean monthly rainfall (mm) averaged over the Congo River Basin from TAMSAT (thick lines) and GPCP (dashed lines) during June 2016–June 2017 (black) and June 2019–June 2020 (red). Pointwise maps of linear regression slope between the monthly **(b)** TAMSAT rainfall anomaly and **(c)** GPCP rainfall anomaly versus DMI in units of $\text{mm } ^\circ\text{C}^{-1}$, with DMI estimated from NOAA ERSST during October for the period 1983–2019. Cross-correlation coefficients (0.51, 0.41) between October DMI and October rainfall anomaly averaged over CRB outlined in black (14°S – 6°N , 13° – 30°E) during 1983–2019 are shown. The Pearson cross-correlation coefficients are computed using detrended timeseries (Supplementary Fig. S6c) and are significant at the 90% confidence level. A standard two-tailed *t*-test is used to test the significance of the cross-correlation coefficients. Location of Kinshasa–Brazzaville station marked (black dot in **b** and **c**).

Measurements at the Kinshasa–Brazzaville station suggest the CRD during October–January are about 40% higher than climatological mean in 2019 (extreme positive IOD year) and 45% lower than the climatology in 2016 (extreme negative IOD year). The total discharge in October–January 2016 is about 69% less as compared to 2019. There is significant lag between variations in the DMI and CRB rainfall as noted above (Supplementary Fig. S6a, b). The CRD integrates rainfall in the Congo basin in both space and time, so the relationship between DMI and CRD at lag times of several months is even stronger than for DMI and CRB rainfall. In particular, there is a lag of about 5 months between the DMI and CRD because of the time it takes for the river system to respond to rainfall variability. The cross correlations at these lags between CRD and DMI are stronger (exceeding 0.5) and more robust than between CRB rainfall and DMI with a correlation of 0.4 (Supplementary Figs. S6a, c and S7a, c). These lags thus represent a source of seasonal predictability for Congo River discharge over west Africa and its effects on ETA near-surface salinity based on the phase of the DMI.

Indian Ocean Dipole affects Atlantic Ocean salinity. The boreal winter discharge from the Congo River is reflected in relatively low sea surface salinity (SSS) along the west African coast as measured from Soil Moisture Active Passive (SMAP)

satellite^{8–10,42} (Fig. 5a, b). The SSS close to the river mouth is modulated by p-IOD and n-IOD events, and was lower by at least 0.8 pss in late 2019 and higher by 0.6 pss in late 2016, relative to the 2015–2020 SSS climatology in the region. Subsequently, SSS continued to drop for three months from December 2019 to March 2020 when the SSS difference reached a maximum of 4 pss between the two years (Fig. 5c, d). Comparing the surface freshwater flux to the local rate of change in SSS suggests that local salinity changes close to the coast were mainly driven by the Congo River outflow⁹ (Fig. 5e, f). Specifically, we find that the SSS drop due to net local surface freshwater flux in this region was less than 0.5 pss during December 2016–March 2017 and December 2019–March 2020, suggesting that salinity changes at the river mouth were mainly related to the Congo River outflow (Fig. 5g). Thus, the unprecedented CRD modulated by the positive Indian Ocean Dipole in 2019 resulted in exceptionally low surface salinity along the ETA coast in contrast to the equally dramatic rise in salinity associated with the strong 2016 n-IOD. Though the satellite SSS record is short, the inverse relationship between DMI and coastal SSS stands out clearly because of the strength of both signals since 2015 (Supplementary Fig. S7b, d).

The freshening of the broader coastal region in ETA was mainly due to the horizontal advection of freshwater discharge from the Congo River which accounts for nearly 80% of the total freshwater supply to the region^{42–45}. The freshwater of CRD forms a salinity

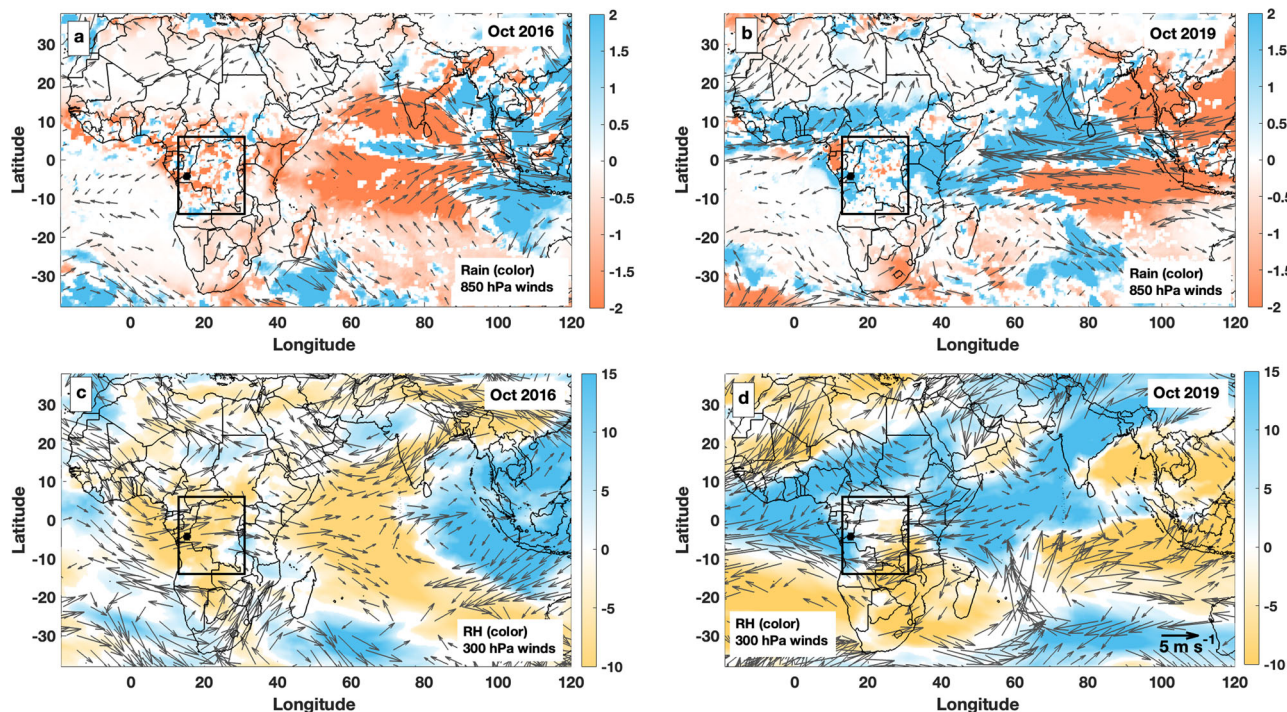


Fig. 3 Upper-tropospheric circulation over Indo-African region during IOD events. Moisture transport weakens over the Congo basin during a negative IOD year (2016) and strengthens during a positive IOD year (2019). GPCP rainfall anomaly (mm day^{-1} ; color) overlaid by ERA5 reanalysis 850 mb wind anomalies (vectors) during October (a) 2016 and (b) 2019. ERA5 reanalysis relative humidity anomaly (percentage; color) at 300 hPa overlaid by ERA5 reanalysis 300 hPa wind anomalies (vectors) during October (c) 2016 and (d) 2019. All the anomaly fields are estimated relative to 1983–2020 climatology. Only values statistically significant at 90% confidence level are shown. Location of Kinshasa–Brazzaville station (black dot) and the Congo River Basin (14°S – 6°N , 13° – 30°E ; black rectangle) are identified in each panel; the 10 m s^{-1} reference wind vector shown in d.

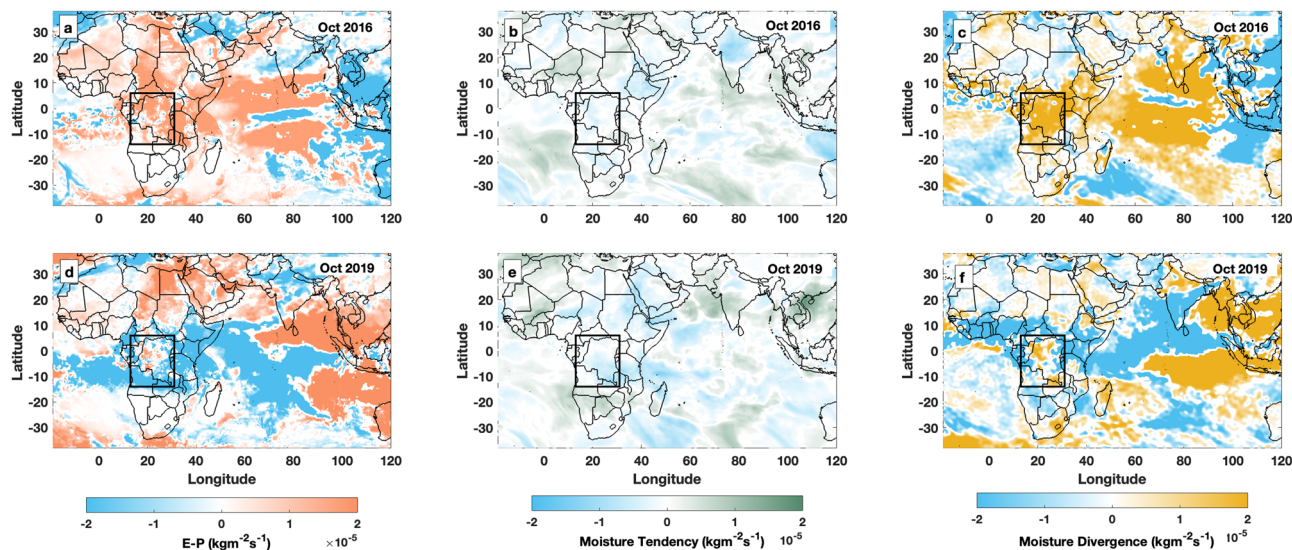


Fig. 4 Atmospheric moisture budget analysis over Indo-African region during IOD events. Atmospheric Moisture Budget anomalies from ERA5 reanalysis during October 2016 and 2019 relative to 1983–2020 climatology. a Total evaporation rate minus precipitation rate anomaly (E-P). Vertically integrated b Moisture tendency anomaly ($\partial q/\partial t$) and c moisture divergence flux ($\nabla \cdot (qv)$) anomaly during October 2016. d–f same as a–c but during October 2019. The anomalies shown are statistically significant at 90% confidence level. All units in $\text{kg m}^{-2} \text{ s}^{-1}$. Location of Kinshasa–Brazzaville station (black dot) and the Congo River Basin (14°S – 6°N , 13° – 30°E ; black rectangle) are shown in c and f.

stratified near-surface layer which restricts coastal upwelling and influences air-sea interaction in eastern Atlantic by aiding the formation of deep barrier layers and warm SSTs^{11,12,43}. Strong near-surface salinity stratification affects the supply of nutrients to the euphotic zone, thus impacting biological productivity, ecosystem dynamics, and fisheries in the coastal waters^{45,46}.

Summary

This study reports for the first time how the Indian Ocean Dipole influences Congo River discharge and surface salinity in the ETA. Although there have been studies which report the relationship between IOD and East and South African rainfall^{20,34}, researchers have just begun to explore the impact of IOD on the rainfall over

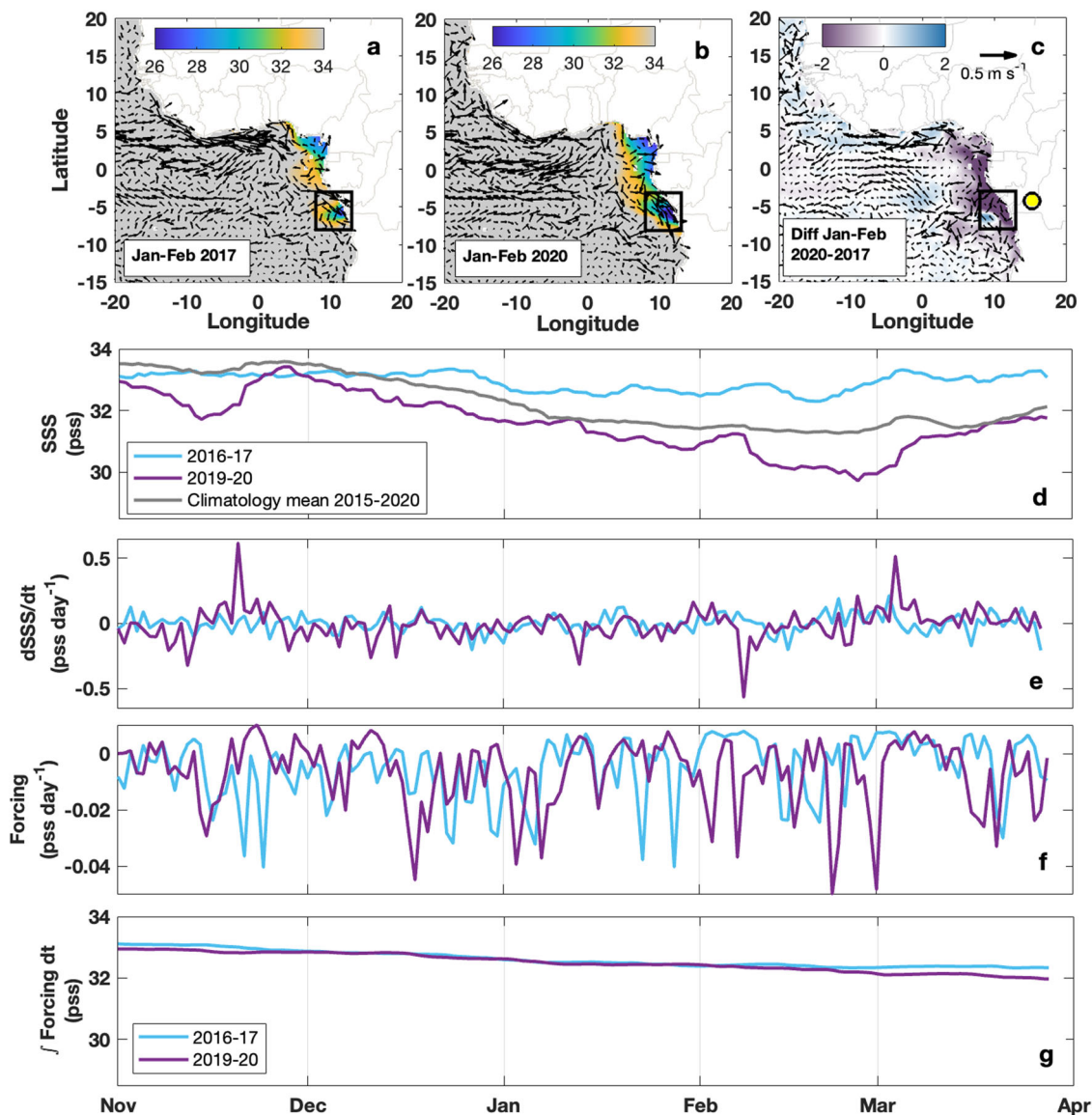


Fig. 5 Effect of the Indian Ocean Dipole on the salinity in the Eastern Tropical Atlantic Ocean. SMAP sea surface salinity (SSS; pss in color) overlaid by AVISO surface geostrophic currents (vectors) averaged during January–February (a) 2017 and (b) 2020. c Difference in January–February mean SSS and surface geostrophic currents between 2020 and 2017. A 0.5 m s^{-1} reference vector is shown. d SMAP SSS (pss) averaged over 4×4 degree box region (4°S – 8°S , 8°E – 12°E) marked in a–c during November–March 2016–2017 (blue), 2019–2020 (purple) and 2015–2020 climatology mean SSS (gray). Timeseries of e rate of change of SSS (pss day^{-1}) shown in panel d, f freshwater forcing term (E–P)/h averaged over the 4×4 box where E is the daily OAF flux evaporation rate (m day^{-1}), P is the daily GPCP precipitation rate (m day^{-1}), S is mean SMAP SSS (pss) and h is the mean mixed layer depth from Argo climatology, (g) time integral of the freshwater forcing term (pss) with added value of surface salinity on 1 November. Timeseries shown in panels d–g are during November–March 2016–2017 (blue) and 2019–2020 (purple).

the Congo Basin³². Here we show that contrasting SST anomalies across the eastern and western Indian Ocean during an IOD event can lead to significant changes in tropospheric circulation, with implications for not only CRB rainfall but Congo River discharge. A detailed atmospheric moisture budget analysis performed using the ERA5 reanalysis shows that the excess precipitation over Congo Basin in 2019 was mainly driven by the moisture divergence related to large-scale circulation changes and the supply of moisture from Indian Ocean during an extreme p-IOD; likewise, the rainfall deficit in 2016 was driven by reduced moisture convergence over the CRB. These moisture fluxes were subsequently reflected in a large CRD increase in 2019 and large CRD decrease in 2016 at the Kinshasa–Brazzaville station one to three months later.

One can also observe the effects of IOD induced changes in CRD on the coastal surface salinity months later from the SMAP satellite. During the extreme p-IOD event in 2019, above normal river discharge contributed to freshening of surface salinity along the coast of west Africa by about 2 pss during December 2019–March 2020 relative to the mean SSS during 2015–2020. On the other hand, during an extreme n-IOD event in 2016, the surface freshening was less than 0.5 pss during the same months due to significant reduction in the Congo River discharge. Thus, the IOD modulates an inter basin transfer of fresh water from the Indian to the Atlantic Ocean. This river discharge in the ETA influences near surface density stratification and the formation of warm barrier layers that affect air-sea interaction and therefore regional weather and climate. These barrier layers also affect

nutrient supply to the euphotic zone, thereby impacting biological productivity, ecosystems, and fisheries in the coastal waters of west Africa^{46,47}. The results we have presented here, illustrated though the extreme contrasts between the 2016 n-IOD and 2019 p-IOD are applicable in more general terms to IOD events of the past several decades based on our statistical analysis of relationships between the DMI, CRB rainfall and Congo River discharge.

As the Indian Ocean warms in response to global warming, the occurrence of extreme p-IOD events is expected to increase²⁴ which can further impact extreme rainfall, flooding and the economic development in Central Africa. The linkage between IOD and Congo River outflow highlighted in this study has implications for flood/drought forecasting and mitigation in the Congo Basin. Moreover, lag relationships between IOD development, Congo River Basin rainfall, river discharge and ocean salinity represent a source of predictability for climate, hydrological and ocean forecasting (Supplementary Figs. S6 and 7). Efforts are underway to improve the predictability of extreme IOD events^{48–51}, but further research is needed to understand the effects of the IOD on the hydrology of the Congo region and its downstream effects on the eastern tropical Atlantic. This can be achieved by improving the existing hydrological and seasonal climate forecast models and conducting fine-scale remote sensing surveys of the surface fresh water from the upcoming Surface Water and Ocean Topography (SWOT) mission by NASA⁵².

Methods

The following datasets have been used in this study to understand the effect between IOD events on Congo River discharge and surface salinity in the Eastern Tropical Atlantic: Daily in situ measurements of discharge measured at Brazzaville/Kinshasa station about 500 km away from the Congo River mouth during January 1954–February 2020. Dipole Mode Index (DMI) is estimated using monthly $2^\circ \times 2^\circ$ resolution NOAA Extended Reconstructed SST (ERSST) V5⁵³ anomalies relative to the 1991–2020 climatology. Monthly relative humidity, 850 hPa and 300 hPa winds, and atmospheric moisture budget terms at 0.25° spatial resolution come from the European Centre for Medium-Range Weather Forecasts (ECMWF) Reanalysis v5 (ERA5)⁵⁴. Daily level 3 sea surface salinity data from the SMAP satellite at 0.25° spatial resolution. Objectively Analyzed air-sea Fluxes (OAFlux)⁵⁵ provide daily 1° gridded rate of evaporation estimates for the global oceans.

We use two different complementary rainfall data sets. Monthly rainfall data during 1983–2020 are available from Tropical Applications of Meteorology using SATellite data and ground-based observations (TAMSAT) at 0.0375° spatial resolution and from the Global Precipitation Climatology Project (GPCP) at 0.5° spatial resolution. TAMSAT has the advantage of higher resolution but it is restricted to land areas only and tends to be noisier because of its higher spatial resolution. GPCP is lower spatial resolution, but a smoother product that covers both land and ocean areas. Comparison of TAMSAT with GPCP over the African continent is shown in Supplementary Figs. S3 and S4.

Nino3.4 index is estimated based on NOAA ERSST V5 relative to the 1991–2020 climatology. To remove El Niño Southern Oscillation (ENSO) effects from the DMI, we used both standard and orthogonal linear regression to remove the Nino3.4 index from DMI SST as shown in Supplementary Fig. S1. The two methods produce about the same result so we opted to apply orthogonal regression throughout our analysis. The correlation between Nino3.4 SST anomaly versus Congo River discharge and Congo basin rainfall is nearly zero, so we do not remove ENSO effects from the discharge and rain.

Atmospheric moisture budget. The atmospheric moisture budget is written as:

$$P + E + \underbrace{\frac{1}{g} \frac{\partial}{\partial t} \int_0^{ps} q dp}_{\text{Term 1}} + \nabla \cdot \underbrace{\frac{1}{g} \int_0^{ps} (qv) dp}_{\text{Term 2}} = 0 \quad (1)$$

where P, E are precipitation and evaporation, g is acceleration due to gravity, q is specific humidity, v is the horizontal wind vector, p is pressure and ps is pressure at the uppermost level of the atmosphere, chosen to be 100 hPa. Term 1 is the tendency of the vertical integral of water vapor in the entire atmospheric column and term 2 describes the divergence of the vertical integral of atmospheric water vapor flux. All units in kilograms per square meter per second ($\text{kg m}^{-2} \text{s}^{-1}$). The atmospheric budget terms in this study are estimated from the ERA5 reanalysis data⁵⁶.

Freshwater forcing. The local freshwater forcing term⁵⁷ over a 4×4 degree region close to Congo River mouth is defined by:

$$\text{Forcing} = (E - P) \frac{S}{h} \quad (2)$$

where P is the rate of precipitation (m day^{-1}) from GPCP, E is the rate of evaporation (m day^{-1}) from OAFlux, S is the mean surface salinity (ps) from SMAP satellite and h is the climatological mean mixed layer depth (m) from the monthly 1° global Argo climatology⁵⁸ averaged over the region.

Data availability

All the datasets are freely available on public domain: Daily in situ measurements of discharge measured at Brazzaville/Kinshasa station obtained from the Global Runoff Data Centre (https://www.bafg.de/GRDC/EN/Home/homepage_node.html). NOAA ERSST at <https://psl.noaa.gov/data/gridded/data.noaa.ersst.v5.html>. Monthly ERA5 data from (<https://www.ecmwf.int/en/forecasts/dataset/ecmwf-reanalysis-v5>). Daily level 3 SMAP sea surface salinity from (<https://www.remss.com/missions/smap/salinity/>). OAFlux daily 1° gridded evaporation rate (http://apdr.csoest.hawaii.edu/dataset/whoi_oafluxday.php). Monthly 1° Mixed layer depth climatology obtained from <http://mixedlayer.ucsd.edu/>. Tropical Applications of Meteorology using SATellite data and ground-based observations (TAMSAT; <https://www.tamsat.org.uk/>) and from the Global Precipitation Climatology Project (GPCP; <https://data.nasa.gov/dataset/GPCP-Precipitation-Level-3-Monthly-0-5-Degree-V3-2/2kyxn57r/data>). Nino3.4 index obtained from <https://psl.noaa.gov/data/timeseries/monthly/NINO34/>.

Code availability

We use basic statistics packages, plotting methods in MATLAB software for the analysis. We do not use any specific code for data processing. The codes used in this study are available upon request to the first author S.J.

Received: 27 March 2023; Accepted: 27 September 2023;

Published online: 10 October 2023

References

- Campbell, D. *The Congo river basin* (pp. 149–165). The World's Largest Wetlands: Ecology and Conservation. (Cambridge University Press, 2005).
- Spencer, R. G. et al. Origins, seasonality, and fluxes of organic matter in the Congo River. *Global Biogeochem. Cycles* **30**, 1105–1121 (2016).
- Vieira, L. H. et al. Unprecedented Fe delivery from the Congo River margin to the South Atlantic Gyre. *Nat. Commun.* **11**, 1–8 (2020).
- Aldorf, D. et al. Opportunities for hydrologic research in the Congo Basin. *Rev. Geophys.* **54**, 378–409 (2016).
- Aufdenkampe, A. K. et al. Riverine coupling of biogeochemical cycles between land, oceans, and atmosphere. *Front. Ecol. Environ.* **9**, 53–60 (2011).
- Sorí, R., Nieto, R., Vicente-Serrano, S. M., Drumond, A. & Gimeno, L. A Lagrangian perspective of the hydrological cycle in the Congo River basin. *Earth Syst. Dyn.* **8**, 653–675 (2017).
- Munzimi, Y. A., Hansen, M. C. & Asante, K. O. Estimating daily streamflow in the Congo Basin using satellite-derived data and a semi-distributed hydrological model. *Hydrol. Sci. J.* **64**, 1472–1487 (2019).

8. Hopkins, J. et al. Detection and variability of the Congo River plume from satellite derived sea surface temperature, salinity, ocean colour and sea level. *Remote Sens. Environ.* **139**, 365–385 (2013).
9. Chao, Y., Farrara, J. D., Schumann, G., Andreadis, K. M. & Moller, D. Sea surface salinity variability in response to the Congo river discharge. *Cont. Shelf Res.* **99**, 35–45 (2015).
10. Martins, M. S. & Stammer, D. Interannual variability of the Congo river plume-induced sea surface salinity. *Remote Sens.* **14**, 1013 (2022).
11. Todd, M. C. & Washington, R. Climate variability in central equatorial Africa: influence from the Atlantic sector. *Geophys. Res. Lett.*, **31**, L23202 (2004).
12. Materia, S., Gualdi, S., Navarra, A. & Terray, L. The effect of Congo River freshwater discharge on Eastern Equatorial Atlantic climate variability. *Clim. Dyn.* **39**, 2109–2125 (2012).
13. Dos Santos, V. et al. Evaluating the performance of multiple satellite-based precipitation products in the Congo River Basin using the SWAT model. *J. Hydrol. Region. Stud.* **42**, 101168 (2022).
14. Laraque, A. et al. Recent budget of hydroclimatology and hydrosedimentology of the congo river in central Africa. *Water*, **12**, 2613 (2020).
15. Saji, N. H., Goswami, B. N., Vinayachandran, P. N. & Yamagata, T. A dipole mode in the tropical Indian Ocean. *Nature* **401**, 360–363 (1999).
16. Webster, P. J., Moore, A. M., Loschnigg, J. P. & Leben, R. R. Coupled ocean–atmosphere dynamics in the Indian Ocean during 1997–98. *Nature* **401**, 356–360 (1999).
17. Yamagata, T. et al. Coupled ocean–atmosphere variability in the tropical Indian Ocean. *Earths Clim. Ocean Atmos. Interact. Geophys. Monogr* **147**, 189–212 (2004).
18. Black, E. The relationship between Indian Ocean sea–surface temperature and East African rainfall. *Philos. Trans. R. Soc. A Math. Phys. Eng. Sci.* **363**, 43–47 (2005).
19. Marchant, R., Mumbi, C., Behera, S. & Yamagata, T. The Indian Ocean dipole—the unsung driver of climatic variability in East Africa. *Afr. J. Ecol.* **45**, 4–16 (2007).
20. Ibebuchi, C. C. Patterns of atmospheric circulation linking the positive tropical Indian Ocean dipole and southern African rainfall during summer. *J. Earth Syst. Sci.* **132**, 13 (2023).
21. Pan, X., Chin, M., Ichoku, C. M. & Field, R. D. Connecting Indonesian fires and drought with the type of El Niño and phase of the Indian Ocean dipole during 1979–2016. *J. Geophys. Res. Atmos.* **123**, 7974–7988 (2018).
22. Cai, W., Cowan, T. & Raupach, M. Positive Indian Ocean dipole events precondition southeast Australia bushfires. *Geophys. Res. Lett.*, **36**, L19710 (2009).
23. Tang, W. et al. Widespread phytoplankton blooms triggered by 2019–2020 Australian wildfires. *Nature* **597**, 370–375 (2021).
24. Cai, W. et al. Opposite response of strong and moderate positive Indian Ocean Dipole to global warming. *Nat. Clim. Change* **11**, 27–32 (2021).
25. Lu, B. et al. An extreme negative Indian Ocean Dipole event in 2016: dynamics and predictability. *Clim. Dyn.* **51**, 89–100 (2018).
26. Lu, B. & Ren, H. L. What caused the extreme Indian Ocean Dipole event in 2019? *Geophys. Res. Lett.* **47**, e2020GL087768 (2020).
27. Santini, M. & Caporaso, L. Evaluation of freshwater flow from rivers to the sea in CMIP5 simulations: insights from the Congo River basin. *J. Geophys. Res. Atmos.* **123**, 10–278 (2018).
28. Pfeiffer, M. et al. Coral Sr/Ca records provide realistic representation of eastern Indian Ocean cooling during extreme positive Indian Ocean Dipole events. *Sci. Rep.* **12**, 10642 (2022).
29. Qiu, Y., Cai, W., Guo, X. & Ng, B. The asymmetric influence of the positive and negative IOD events on China’s rainfall. *Sci. Rep.* **4**, 4943 (2014).
30. Bola, G. B. et al. Multi-return periods, flood hazards, and risk assessment in the Congo River Basin. In: Congo Basin hydrology, climate, and biogeochemistry: a foundation for the future, 519–540 (AGU Wiley, 2022).
31. Ogwang, B. A., Ongoma, V., Xing, L. & Ogou, K. F. Influence of Mascarene high and Indian Ocean dipole on East African extreme weather events. *Geograph. Pannonica* **19**, 64–72 (2015).
32. Moihamette, F., Pokam, W. M., Diallo, I. & Washington, R. Extreme Indian Ocean dipole and rainfall variability over Central Africa. *Int. J. Climatol.* **42**, 5255–5272 (2022).
33. Bahaga, T. K., Mengistu Tsidu, G., Kucharski, F. & Diro, G. T. Potential predictability of the sea-surface temperature forced equatorial East African short rains interannual variability in the 20th century. *Q. J. R. Meteorol. Soc.* **141**, 16–26 (2015).
34. Funk, C. et al. Examining the role of unusually warm Indo-Pacific sea-surface temperatures in recent African droughts. *Q. J. R. Meteorol. Soc.* **144**, 360–383 (2018).
35. Lüdecke, H. J., Müller-Plath, G., Wallace, M. G. & Lüning, S. Decadal and multidecadal natural variability of African rainfall. *J. Hydrol. Region. Stud.* **34**, 100795 (2021).
36. Wainwright, C. M., Finney, D. L., Kilavi, M., Black, E. & Marsham, J. H. Extreme rainfall in East Africa, October 2019–January 2020 and context under future climate change. *Weather* **76**, 26–31 (2021).
37. Ficchi, A. et al. Beyond El Niño: unsung climate modes drive African floods. *Weather Clim. Extremes* **33**, 100345 (2021).
38. MacLeod, D., Graham, R., O’Reilly, C., Otieno, G. & Todd, M. Causal pathways linking different flavours of ENSO with the Greater Horn of Africa short rains. *Atmos. Sci. Lett.* **22**, e1015 (2021).
39. Anderson, W. et al. Multiyear la niña events and multiseason drought in the horn of africa. *J. Hydrometeorol.* **24**, 119–131 (2023).
40. Ratna, S. B., Cherchi, A., Osborn, T. J., Joshi, M. & Uppara, U. The extreme positive Indian Ocean dipole of 2019 and associated Indian summer monsoon rainfall response. *Geophys. Res. Lett.* **48**, e2020GL091497 (2021).
41. Kitambo, B. et al. A combined use of in situ and satellite-derived observations to characterize surface hydrology and its variability in the Congo River Basin. *Hydrol. Earth Syst. Sci.* **26**, 1857–1882 (2022).
42. Bingham, F. M., Brodnitz, S. & Yu, L. Sea surface salinity seasonal variability in the tropics from satellites, gridded in situ products and mooring observations. *Remote Sens.* **13**, 110 (2020).
43. Dossa, A. N., Da-Allada, C. Y., Herbert, G. & Bourlès, B. Seasonal cycle of the salinity barrier layer revealed in the northeastern Gulf of Guinea. *Afr. J. Marine Sci.* **41**, 163–175 (2019).
44. Camara, I., Kolodziejczyk, N., Mignot, J., Lazar, A. & Gaye, A. T. On the seasonal variations of salinity of the tropical Atlantic mixed layer. *J. Geophys. Res. Oceans* **120**, 4441–4462 (2015).
45. Awo, F. M. et al. Seasonal cycle of sea surface salinity in the Angola upwelling system. *J. Geophys. Res. Oceans* **127**, e2022JC018518 (2022).
46. Tchupalanga, P. et al. Eastern boundary circulation and hydrography off Angola: building angolan oceanographic capacities. *Bull. Am. Meteorol. Soc.* **99**, 1589–1605 (2018).
47. Ostrowski, M., Da Silva, J. C. & Bazik-Sangolay, B. The response of sound scatterers to El Niño-and La Niña-like oceanographic regimes in the southeastern Atlantic. *ICES J. Marine Sci.* **66**, 1063–1072 (2009).
48. Zhao, S., Jin, F. F. & Stuecker, M. F. Improved predictability of the Indian Ocean Dipole using seasonally modulated ENSO forcing forecasts. *Geophys. Res. Lett.* **46**, 9980–9990 (2019).
49. Feba, F., Ashok, K., Collins, M. & Shetye, S. R. Emerging skill in multi-year prediction of the Indian Ocean Dipole. *Front. Clim.* **3**, 736759 (2021).
50. Doi, T., Behera, S. K., & Yamagata, T. (2022). On the predictability of the extreme drought in East Africa during the short rains season. *Geophys. Res. Lett.* **49**, e2022GL100905.
51. Liu, M., McPhaden, M. J., Ren, H.-L., Balmaseda, M. A. & Wang, R. Oceanic heat content as a predictor of the Indian Ocean Dipole. *J. Geophys. Res. Oceans* **127**, e2022JC018896 (2022).
52. Huang, Q., Long, D., Du, M., Han, Z. & Han, P. Daily continuous river discharge estimation for ungauged basins using a hydrologic model calibrated by satellite altimetry: implications for the SWOT mission. *Water Resour. Res.* **56**, e2020WR027309 (2020).
53. Huang, B. et al. Extended reconstructed sea surface temperature, version 5 (ERSSTv5): upgrades, validations, and intercomparisons. *J. Clim.* **30**, 8179–8205 (2017).
54. Hersbach, H. et al. The ERA5 global reanalysis. *Q. J. R. Meteorol. Soc.* **146**, 1999–2049 (2020).
55. Yu, L. & Weller, R. A. Objectively analyzed air–sea heat fluxes for the global ice-free oceans (1981–2005). *Bull. Am. Meteorol. Soc.* **88**, 527–540 (2007).
56. Mayer, J., Mayer, M. & Haimberger, L. Consistency and homogeneity of atmospheric energy, moisture, and mass budgets in ERA5. *J. Clim.* **34**, 3955–3974 (2021).
57. Cronin, M. F., Pelland, N. A., Emerson, S. R. & Crawford, W. R. Estimating diffusivity from the mixed layer heat and salt balances in the North Pacific. *J. Geophys. Res. Oceans* **120**, 7346–7362 (2015).
58. Holte, J., Talley, L. D., Gilson, J. & Roemmich, D. An Argo mixed layer climatology and database. *Geophys. Res. Lett.* **44**, 5618–5626 (2017).

Acknowledgements

This research was performed while the first author S.J. is a National Research Council (NRC) postdoctoral fellow at the National Oceanic and Atmospheric Administration (NOAA) Pacific Marine Environmental Laboratory (PMEL) in Seattle, Washington. M.J.M. is funded by NOAA. The authors thank NRC and NOAA for supporting with this work. This is PMEL contribution no. 5456. We thank the anonymous reviewers for providing constructive feedback during the review process.

Author contributions

S.J. contributed to conceptualization, data curation, methodology, validation, data visualization and writing the original draft. M.J.M. contributions include project administration, investigation, supervision, reviewing, editing the manuscript.

Competing interests

The authors declare no competing interests.

Additional information

Supplementary information The online version contains supplementary material available at <https://doi.org/10.1038/s43247-023-01027-6>.

Correspondence and requests for materials should be addressed to Sreelekha Jarugula.

Peer review information *Communications Earth & Environment* thanks Chibuikwe Chiedozie Ibebuchi and Moses A Ojara for their contribution to the peer review of this work. Primary Handling Editors: Heike Langenberg. A peer review file is available

Reprints and permission information is available at <http://www.nature.com/reprints>

Publisher's note Springer Nature remains neutral with regard to jurisdictional claims in published maps and institutional affiliations.



Open Access This article is licensed under a Creative Commons Attribution 4.0 International License, which permits use, sharing, adaptation, distribution and reproduction in any medium or format, as long as you give appropriate credit to the original author(s) and the source, provide a link to the Creative Commons license, and indicate if changes were made. The images or other third party material in this article are included in the article's Creative Commons license, unless indicated otherwise in a credit line to the material. If material is not included in the article's Creative Commons license and your intended use is not permitted by statutory regulation or exceeds the permitted use, you will need to obtain permission directly from the copyright holder. To view a copy of this license, visit <http://creativecommons.org/licenses/by/4.0/>.

© The Author(s) 2023